Diamond Milling with Multiple Cutting Edges

Lars Schönemann, Oltmann Riemer, and Ekkard Brinksmeier

Abstract Ultra-precision milling with multiple diamond cutting edges—which generally is favorable in terms of economic efficiency—requires an in-process tool setting system that allows for the compensation of alignment and fixation errors. Such a system was designed on the basis of thermal expansion as the main means of actuation. The heat input is generated by infrared light diodes which feed the respective energy to the rotating tool contactlessly. It is controlled in a way that ensures that only a specific portion of the tool holder is illuminated and therefore thermally expanded. By measuring the displacement at a reference plane with a capacitive measurement system and feeding it back to the control system, the actual position of the diamond cutting edge can be precisely set in nanometer range. This chapter gives an overview on the main technical developments for the respective prototype system and presents its performance when used in a machining environment.

1 Surface Generation in Diamond Milling

In general, ultra-precision machining with diamond tools (UP-machining) is an indispensable technology of optics manufacturing [6]. UP-milling processes, in particular, allow for the direct generation of complex geometries and freeform shapes with extremely smooth surface roughness and high form accuracy [7, 21]. The economic viability of these technologies is often increased by applying them in replication processes, e.g. by diamond machining the required molds for plastic or glass optics production [4, 18]. With this it is possible to manufacture a large quantity of optical parts from a single master form. Although comparably long processing times are acceptable in this case, the duration of diamond milling an optical mold is still a bottleneck in production, because the machining may require several minutes even for geometrically simple parts and up to multiple hours or even days for complex geometries [3].

L. Schönemann (✉) · O. Riemer · E. Brinksmeier
Leibniz Institute for Materials Engineering IWT, Bremen, Germany
e-mail: schoenemann@iwt.uni-bremen.de

MAPEX Center for Materials and Processes, University of Bremen, Bremen, Germany

E. Brinksmeier and L. Schönemann (eds.), *Ultra-precision High Performance Cutting*,
Lecture Notes in Production Engineering, https://doi.org/10.1007/978-3-030-83765-5_2

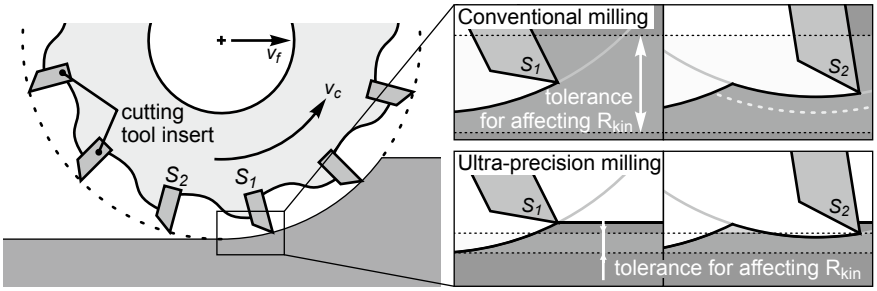

Fig. 1 Engagement conditions for multiple cutting edges in conventional and ultra-precision machining, cf. [11]

One of the reasons for these exceptionally long machining times is the limitation of diamond milling processes to the application of only one single cutting edge. Hence, these processes are also named "fly-cutting". The challenge of utilizing multiple cutting edges in diamond milling is their adjustment to achieve equal and predictable engagement conditions. Upon mounting the tool insert[1] on the tool holder, the manufacturing and assembly tolerances inevitably yield a deviation in fly-cut radius (Δr_{fly}), axial position (Δs, i.e. the subsequent cutting edges not running in the same "track"), and also in engagement angle ($\Delta\alpha$, $\Delta\gamma$). In particular, the axial and radial deviations may yield a magnitude of several micrometers.

Simply speaking, only if the fly-cut radii of all cutting edges feature a maximal difference below the kinematic roughness (in optics machining this typically implies $R_{kin} < 10$ nm), such a setup may be reliably used for machining (Fig. 1).

In reality, however, the associated surface generation is much more complex. When brought into contact with the workpiece, the radial and axial deviation of the cutting tools cause an irregular surface pattern which requires more describing parameters than just the simple formula to approximate the kinematic roughness in fly-cutting ($R_{kin} = f^2/(8r_\varepsilon)$). Instead, the differences in fly-cut radius Δr_{fly}, in axial direction Δs as well as all other geometric deviations such as the differences in shape and waviness of the cutting edge and the relative orientation of the cutting inserts have to be considered. A detailed analysis in 2D, i.e. for the kinematic roughness, can be found in [15]. A 3D-analysis of the generated surface is possible with numerical approaches, as presented in [16] and [17]. Ultimately, even the slightest deviation in any of these parameters results in new surface patterns that are generated and will lead to an undetermined surface roughness compared to fly-cutting with a single cutting edge (Fig. 2).

In summary, all cutting edges have to be aligned with as much precision as possible. The radial deviation Δr_{fly} has to be at least smaller than the maximum undeformed chip thickness $h_{cu,max}$ of the process, for all cutting edges to be involved in the material removal. Preferably, the remaining deviation of all cutting edges has to

[1] usually a carbide insert with a diamond soldered on top; the diamond is ground and lapped to form the actual cutting edge.

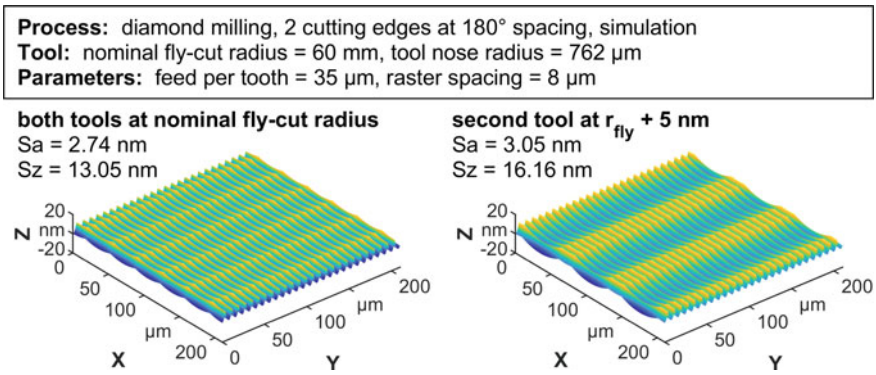

Fig. 2 Simulated surface of a two-tool diamond milling process with and without a deviation in fly-cut radius [17]

be lower than the kinematic roughness R_{kin}, i.e. <10 nm, in order to generate the final surface topography.

2 Tool Adjustment for Diamond Milling

For the compensation of positioning and guidance errors in machine tools, mechatronic components are applied to an increasing degree [8]. Despite the current progress of these technologies, the transferal of conventionally utilized concepts for tool alignment to ultra-precision machining is particularly challenging, as these systems should affect the general machining performance as little as possible. Thus, a combination of flexure hinges and highly precise actuators is commonly chosen [1, 19]. Implementing such alignment systems in milling operations, however, features the additional challenge of the milling tool rotating at high speeds on an air bearing. As a consequence, a lot of effort has to be put into the energy supply and data transfer systems, which ideally need to work contactless (for not disturbing the runout of the spindle) and be as lightweight and compact as possible (for maximizing the dynamics of the process). Systems that have been previously designed were not able to meet all of these requirements. The prototypes presented in [2] and [20] are based on purely mechanical tool setting and thus were not able to achieve the required tool setting precision. The mechatronic device presented in [9] achieves this, but is exceptionally voluminous and heavy due to the inclusion of wireless transmitters and control components on the rotor. This affects the spindle performance negatively and makes it effectively unusable for ultra-precision milling of optical surfaces.

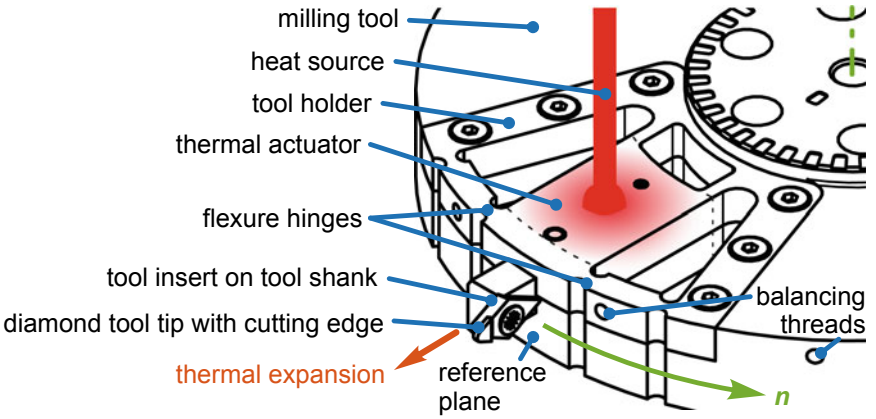

Fig. 3 Principle of an adjustable tool holder for generating a radial tool shift by thermal expansion [17]

2.1 Concept of Thermal Tool Adjustment

In the presented research work, the concept of defined thermal expansion was applied. This means that a specific portion of the tool holder is locally heated in order to expand it in radial direction (Fig. 3). Thereby, the tool that is fixed at the end of this "thermal actuator" changes its effective cutting radius. Using a dedicated control of the heat input, the expansion can be controlled in a way that the deviation between the subsequent cutting edges is minimized.

For minimizing the impact on the dynamic performance of the fly-cutter, e.g. the maximum spindle speed or the induced unbalances, the number of mechanical parts and electrical components that have to be integrated on the rotor has to be as low as possible. Heat input can be generated without mechanically contacting the substrate, e.g. by infrared radiation. This offers the unique possibility to place all heat-generating equipment on the static side of the fly-cutting process. In consequence, only very few mechanical parts are required on the rotor.

The required heat input may be calculated on the basis of material parameters and physical correlations. Thus, a mathematical model can be derived and used in the closed loop control of the thermal expansion. Moreover, thermal processes generally are elapsing slowly and thus, a specific thermal state can be maintained easily over a relatively long time by feeding only a minimum amount of heat into the system. This further facilitates the closed loop control. Thereby, it has to be ensured that the system is capsuled in the machine tool so that the delicate thermal state is not affected by coolant and forced convection due to the spindle rotation. This solution also ensures that the thermal state of the actuator does not affect the overall thermal stability of the machine tool. Generally, as only a small expansion of several nanometers is required, the proposed concept should not have a major effect on this issue.

Table 1 Calculations for thermal expansion and heating time

Actuator: steel 42CrMo4, $V = 10 \times 10 \times 30\ mm^3$				
$\alpha = 11.1$ nm mm^{-1} K^{-1}, $\rho = 7.850 \times 10^{-3}$ g mm^{-3}, $c_p = 461$ J kg^{-1} K^{-1}, $\eta = 0.4$				
ΔL	ΔT	Q	P	t_{heat}
10 nm	0.03 K	0.33 J	0.5 W 10 W	1.63 s 0.08 s
3.33 µm	**10 K**	108.57 J	0.5 W 10 W	542.83 s 27.16 s

2.2 Determination of Required Heat Input

Before actually designing holding mechanism for the tool inserts, the concept was validated, both analytically and numerically. A first approximation of the required heat input can be calculated by the standard physical equation of thermal expansion that takes the base length of a beam L_0, the coefficient of thermal expansion of the substrate α and temperature difference ΔT into account (Eq. 1).

$$\Delta L = \alpha \cdot L_0 \cdot \Delta T \tag{1}$$

Given the size of a typical fly-cutter to be approximately 150 mm in diameter, including a $L_0 = 30$ mm sized actuator into this seems reasonable. With the coefficient of thermal expansion being $\alpha \approx 11.1$ nm mm^{-1}K^{-1} for a 42CrMo4 type steel, the required temperature change for a $\Delta L_{min} = 10$ nm calculates to $\Delta T_{min} \approx 0.03$ K. On the other end, the maximum tolerable temperature change is set to $\Delta T_{max} = 10$ K above ambient. This yields a total thermal expansion of $\Delta L_{max} = 3{,}33$ µm.

In order to determine the required heat input Q for such a thermal expansion, the mass $m = v \times \rho$ and the thermal capacity c_p of the actuator have to be considered (Eq. 2).

$$Q = c_p \cdot v \cdot \rho \cdot \Delta T \tag{2}$$

Knowing the required heat input, it is possible to calculate the heating time t_{heat} required by a heat source with a power P and the thermal absorption η of the actuator surface (Eq. 3).

$$t_{heat} = \frac{Q}{\eta \cdot P} \tag{3}$$

In the following Table 1, the heat input and heating time for ΔL_{min} and ΔT_{max} is calculated for two kinds of heat sources, a laser with $P_{\text{Laser}} = 10$ W and an infrared-light emitting diode (IR-LED) with $P_{LED} = 0.5$ W. The calculation shows that the required expansion can be theoretically reached by both sources, though at different heating times.

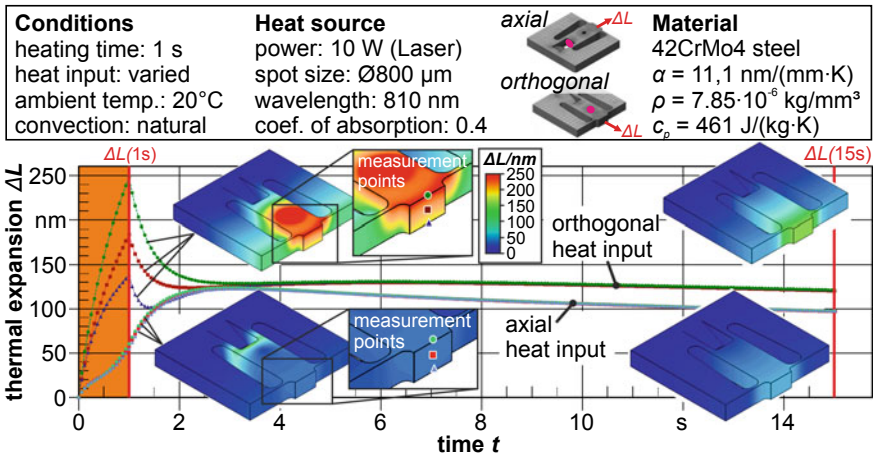

Fig. 4 Thermal expansion for heating an orthogonally and axially coupled thermal actuator with a Laser source ($P_{\text{Laser}} = 10$ W)

For the further analysis of the heat distribution and the 3D elongation of the material, numerical calculations were conducted using "Autodesk Simulation Mechanical 2016". Here, the actuator was modeled as a beam of the aforementioned size which was integrated into a setup for experimental verification. Therefore, the beam was connected to the base by two struts at the rear and two flexure hinges at the front. The setup offers two different setups for the coupling of the heat source: first, an orthogonal coupling in which the heat source is directed to the top (and possibly also the bottom) face of the actuator. Second, an axial coupling in which the heat is introduced to the rear face of the actuator. With the simulations it was investigated whether the orthogonal or axial coupling is preferable for a symmetric expansion and also if a high power (Laser) or low power (IR-LED) heat source is sufficient. For the simulation, the heat input was limited to a 1 s burst for all experiments.

The resulting expansion of heating the actuator by a Laser source is shown in Fig. 4.

Due to the high costs and complexity of integrating a Laser source in such a setup, the orthogonal coupling is limited to be one-sided, i.e. only on the top face of the actuator. This results in a tiling of the front face (at which the tool would be mounted) due to the inhomogeneous heat distribution within the actuator that is visible as a deviation in expansion of the three test points. After switching off the light source, this deviation is quickly reduced to a minimum as the heat distribution and thus the expansion becomes more homogeneous. Overall, an elongation of around $\Delta L = 125$ nm can be achieved without tilting after about 3 s in total using the orthogonal coupling. In contrast, the axial coupling shows a more homogeneous heat distribution from the start, as this setup serves the symmetry of the actuator. Furthermore, it is noticeable that the expansion of the actuator continues even after switching off the Laser due to the spreading of the heat (thermal conduction). After

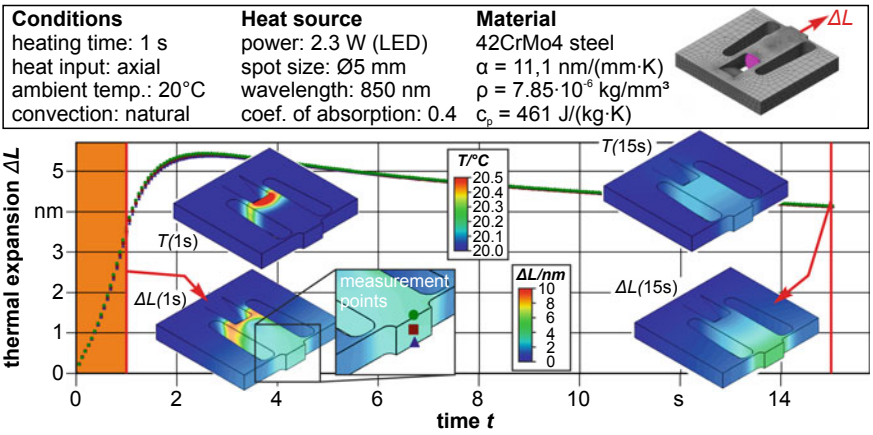

Fig. 5 Thermal expansion for heating an axially coupled thermal actuator with a IR-LED source ($P_{\mathrm{LED}} = 0.5$ W)

3 s of simulated time, the thermal expansion reaches a similar extent than that of the orthogonal coupling. However, the heat is dissipated more quickly in this case and therefore, the thermal expansion also decreases thereafter. Nevertheless, an expansion of 100 nm is still measurable after 15 s in total.

The simulated expansion for using an IR-LED with $P_{\mathrm{LED}} = 0.5$ W as heat source and axial coupling is shown in Fig. 5. The simulation shows that such a LED is capable of achieving an elongation in the nanometer range with a 1 s burst. The maximum expansion is again reached after 3 s of simulated time and measures about $\Delta L = 5.5$ nm. This implies that such an IR-LED might well be sufficient for driving the thermal actuator for the intended purpose of nanometer-precise tool setting. The benefit of this solution would be that a two-sided orthogonal setup could be realized as well, because LED are inexpensive and easy to integrate (both electrically and concerning operator safety).

In addition to the simulations with 42CrMo4 steel, the performance of other steel types has been evaluated as well. In particular, the stainless steel X40Cr14 has proven to deliver an increased thermal expansion (Fig. 6), because of its lower thermal conductivity ($\kappa_{\mathrm{X40Cr14}} = 22.6$ W m^{-1} K^{-1} vs. $\kappa_{\mathrm{42CrMo4}} = 42.6$ W m^{-1} K^{-1}).

2.3 *Validation of the Thermal Mechanism in a Static Test Setup*

The concept of a thermal actuator was first evaluated in a static test setup. This offered the possibility to minimize the distortion from the rotation of the spindle (noise, centering and roundness error of the reference plane) and also facilitated the

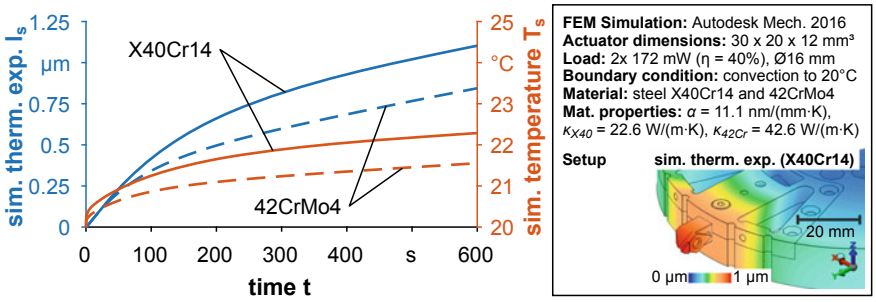

Fig. 6 Comparison of maximum temperature and thermal expansion for 42CrMo4 and X40Cr14 type steel

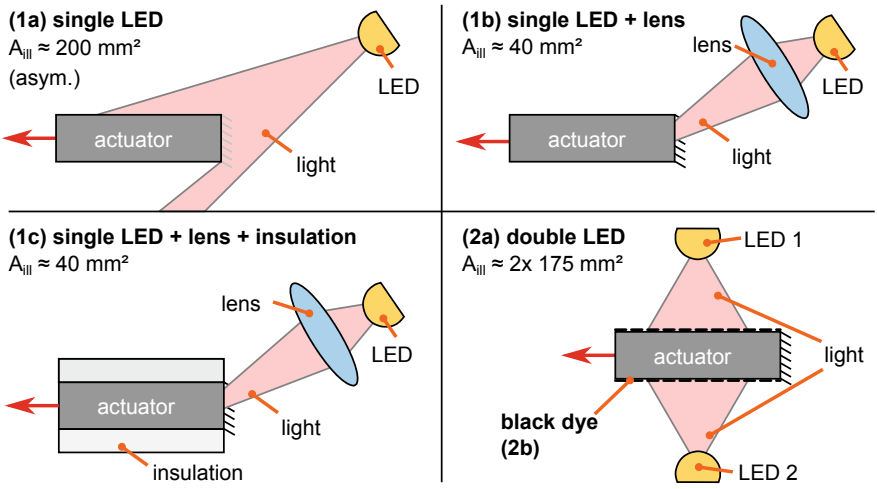

Fig. 7 Configurations of the static test stand for evaluating the thermal actuating principle

test of different heating setups. Four configurations were analyzed in this study: (1a) the illumination of the actuator's rear face with a single LED, (1b) the focusing of the LED radiation on the rear face with an additional lens, (1c) the addition of an insulating layer on the top and bottom face of the actuator to prevent heat loss by convection, and (2a) the illumination of both the top and bottom face of the actuator with two separate LED heat sources. The latter test was repeated with an additional coloring of the actuator faces with black ink (2b) to maximize the heat absorption (Fig. 7).

The results in Fig. 8 indicate that using only a single LED that is directed at the back of the actuator generates a thermal expansion of only ≈250 nm, which is not sufficient. Focusing the light does not generate a positive effect, but reduces the achievable expansion to slightly below 200 nm, which is probably caused by the absorption of the infrared radiation within the added lens. Isolating the actuator

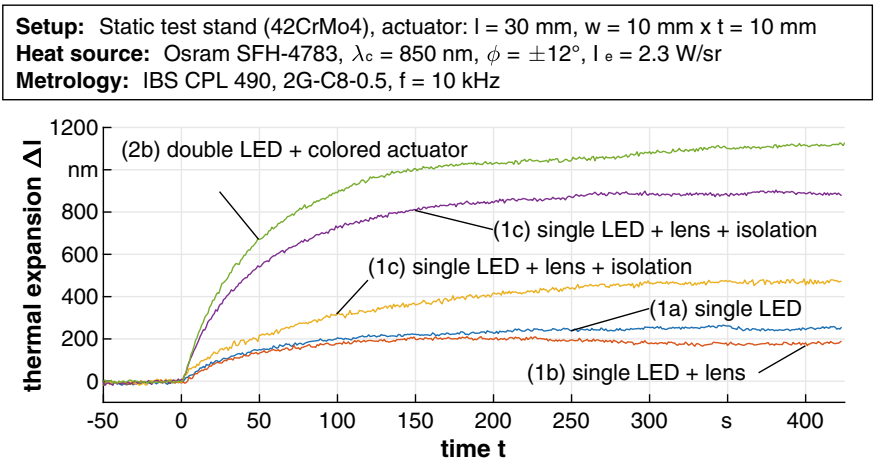

Fig. 8 Step response of the static test stand for the selected configurations

almost doubles the achievable expansion to about 470 nm. The best results can be achieved by using the double-sided LED setup that without any further modifications generates an expansion of 870 nm. When adding a black coloring to the illuminated actuator faces, the heat input is increased further, yielding an expansion of more than 1,100 nm.

Overall, these tests have shown that the general concept of using thermal expansion for tool setting in the nanometer range is basically applicable.

3 Determination of Tool Holder Geometry

The geometry of the actuator has been integrated into the design of a tool holder for diamond milling with two tools. As it is obvious from the calculations and simulations, a thermal tool setting mechanism would achieve the required precision, but with the given constraints on maximum temperature clearly lacks the capacity to achieve a maximal stroke that would suffice the typical tolerances of diamond tool inserts. Therefore, the thermal actuator was extended by a mechanical pre-setting mechanism for a coarse alignment of the cutting edges to the range of the thermal expansion. A detailed description of the initial designs can be found in [10]. These featured a mechanical mechanism that was mounted as an additional component at the front of the thermal actuator. Due to reasons of stability and overall size of the tool holder, this concept was discarded and replaced by an internal mechanism as an integral part of the thermal actuator. This novel design was first presented in [14] and later in more detail in [15].

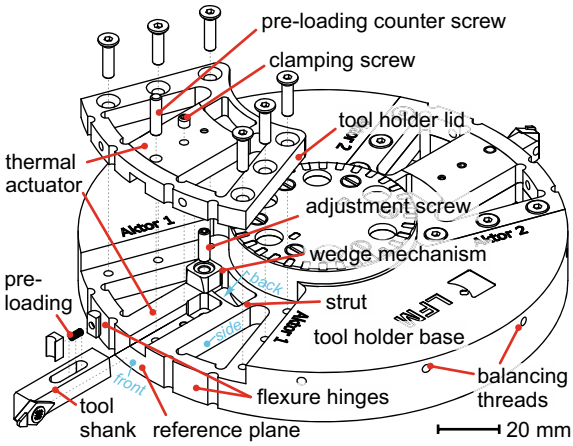

Fig. 9 Final design of a tool holder with two thermal actuators

Table 2 Technical data of tool holder and thermal actuator

Nominal engagement radius r_{fly}	65 mm
Number of actuators n_{act}	2
Spacing of actuators χ_{act}	180°
Dimensions of actuator $l \times w \times h$	$30 \times 20 \times 12$ mm^3
material	Steel X40Cr14
Thermal conductivity κ	22.6 W m^{-1} K^{-1}
Coef. of thermal expansion α	11.1 µm m^{-1} K^{-1}
Coef. of thermal absorption η	≈40%

The final design was made for a tool holder with a nominal diameter of 130 mm and features two beam-like thermal actuators (i.e. two tools) at 180° spacing which can potentially be increased up to four (Fig. 9). Each of the actuators is connected to the base of the tool holder by two struts at the rear and two flexure hinges at the front side while the rest is cut away to minimize thermal conduction to the base. The total dimensions of the actuator are 30 mm in length, 20 mm in width and 12 mm in thickness. The substrate material of the tool holder is X40Cr14 type steel which has shown the most promising results in the simulations. All relevant data are comprised in Table 2.

The mechanical presetting mechanism has been integrated into the thermal actuator and now features the tool shank as a slide. The tool shank is preloaded against a wedge mechanism with a 5° angle. When this wedge is moved by a precision screw, it shifts the tool shank in radial direction with a transmission ratio of $\tan(5°) = 0.0874$. In this way, the tool insert can be positioned across a range of ≈180 µm with a precision of <1 µm (Fig. 10) which is sufficient to compensate for all deviations from fixation.

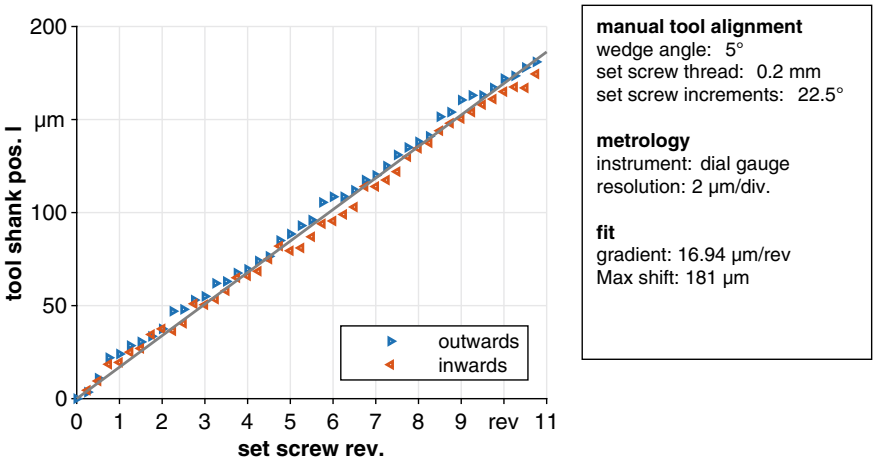

Fig. 10 Performance of mechanical presetting mechanism

4 Design of a Contactless Heat Input System for a Rotating Actuator

In a static setup, the heat input to the actuator is very simple, as both the heat source and the actuator remain at a fixed position. In contrast, the tool and hence also the actuator are rotating at several hundred revolutions per minute in an actual milling process. The heat transfer via an IR-LED is contactless per se and thus does not raise a problem here. However, the LED has to remain at a fixed position or otherwise the system design would get very complex. Thus, the heat can only be transferred to the actuator within a small timeframe, which is defined by the width of the actuator, circumference on which it is rotating and the spindle speed (Eq. 4).

$$t_{heat,rev} = \frac{w}{2 \cdot \pi \cdot r_{\text{act}} \cdot n/60} \tag{4}$$

At a typical spindle speed for diamond fly-cutting of $n = 1{,}000\ \text{min}^{-1}$, this calculates to $t_{heat,rev} = 4$ ms whereas for high speed cutting at $n = 20{,}000\ \text{min}^{-1}$ it is only $t_{heat,rev} = 200\ \mu\text{s}$. In combination with the forced convection due to the rotation, this timespan is not enough to generate a stable elevated temperature of the actuator. As a consequence, a device that allows the heat input to follow the actuator movement has to be devised.

A moving ring light system (patent pending) has been developed to serve this purpose [13]. It consists of multiple LEDs that are evenly distributed along a circle in a way that the peak intensity is directed at the actuator midpoint. All LED are powered by a common energy supply and each LED can be activated by a dedicated transistor, i.e. by a low-power signal line. One or more of these LED are used to

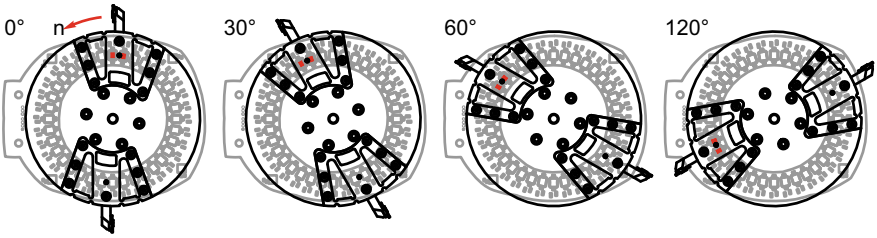

Fig. 11 Principle of the ring light system for a quasi-continuous heating of the thermal actuator. LEDs advance according to the angular position of the target actuator

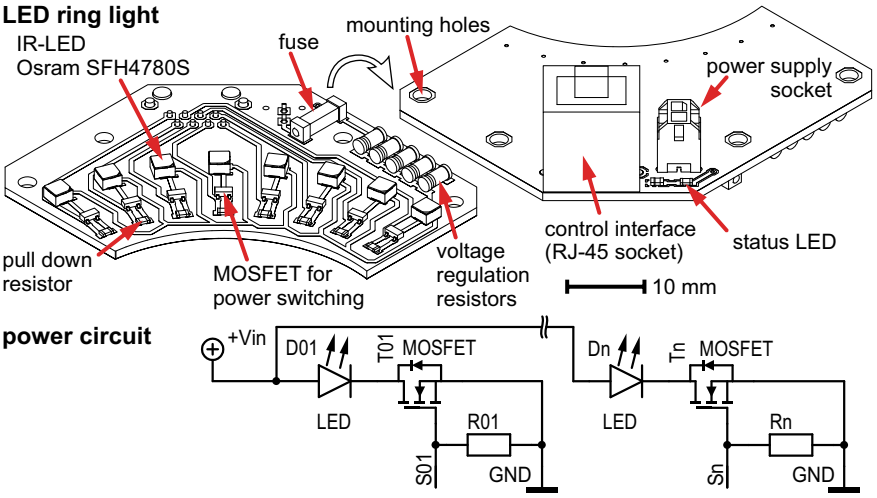

Fig. 12 Ring light (1/4) with 8 IR-LED, switching transistors and common power supply for all LED

illuminate the thermal actuator while the other LED are switched off. Upon rotation of the milling tool, the active LED are advanced along the ring to follow the position of the actuator (Fig. 11), while the body of the ring light stays stationary. In this way, a quasi-constant heating of the actuator is achieved.

For reasons of simplicity, handling and manufacturability, the current ring light system consists of four equal segments that cover a quarter of the ring and incorporate 8 IR-LED each (Fig. 12). In this way, the ring light can be easily dismounted even when enclosing the spindle shaft for illuminating the backside of the actuator. All technical specifications of the ring light systems are comprised in Table 3.

The switching of the LED is performed by a dedicated control electronics which was designed as a shield circuit board for an Arduino Mega 2560 board (Fig. 13). The Arduino evaluates the angular position of the spindle, either directly via the spindle encoder or via photo sensors that detect a scale on the tool holder, and generates the appropriate sequence of activated LED. As the use of LED also enables the

Table 3 Technical specifications of ring light system

Total number of LED	32
Element shape	¼ ring
IR-LED per element	8
IR-LED manufacturer and model	Osram SFH 4780S
Wavelength λ	820 nm
Radiant intensity I_e	2.3 W sr^{-1}
Half-angle φ	$\pm 10°$
Total radiant flux Φ_e	600 m W
Rise time t_r	8 ns
Fall time t_f	14 ns
Forward voltage U_f	3.3 V
Forward current I_f	0.5 A

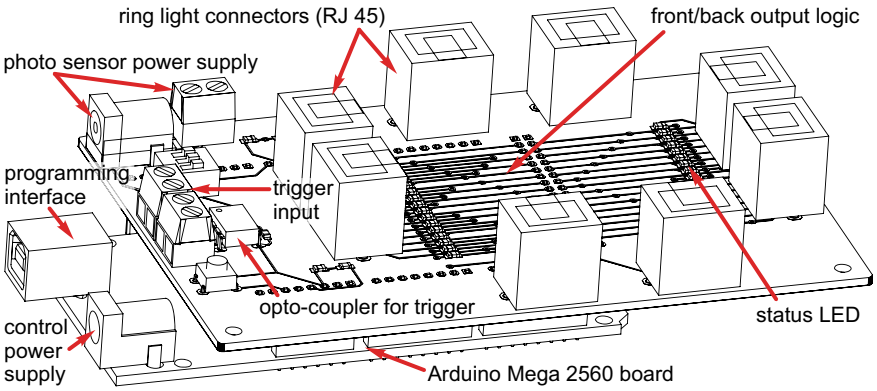

Fig. 13 Circuit board (Arduino Shield) for ring light control

application of double-sided heating, two separate sequences need to be generated for the front and back ring light, as one of them is running clockwise and the other one counter-clockwise to follow the spindle rotation. This is directly done on the circuit board by a hard-wired logic.

5 Experimental Spindle Setup for Tool Holder Evaluation

The evaluation of the finalized thermal tool holder was mainly conduced on two experimental platforms. First, an air-cutting spindle test stand was used on which the tool holder can be analyzed without cutting interaction (Fig. 14).

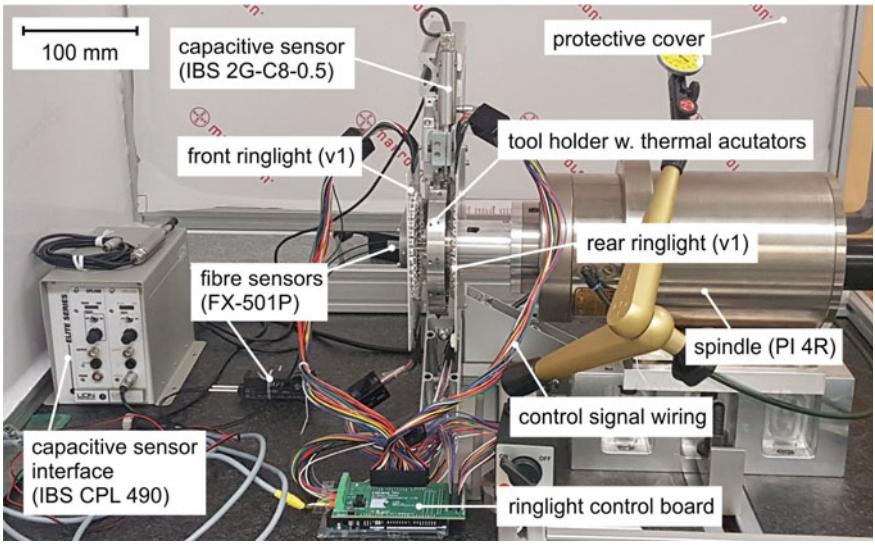

Fig. 14 Offline test stand for evaluating the thermal tool holder on an air-bearing spindle without cutting interaction

It consists of a Professional Instruments 4R air-bearing spindle on which the milling tool incorporating the thermal tool holder is fixed using an adapter which provides the needed clearance for mounting the rear ring light. Furthermore, a fiber sensor (FX-501P by Panasonic) is used to monitor the revolution of the actuator and determine the angular position for advancing the LED. The expansion is evaluated by measuring the position reference plane located below the tool shank on the circumference of the tool holder with a capacitive sensor (IBS 2G-C8-0.5 with a CPL 490 interface).

This setup was later transferred to a Nanotech 500FG machine tool for additional cutting experiments. The 4R air-bearing spindle is mounted on the B-axis table of the machine tool while the workpiece is fixed on the (clamped) main spindle of the 500FG. In addition to the test stand, a dynamometer was placed under the workpiece fixture to be able to measure the development of cutting forces during machining and to correlate this to the thermal expansion. The setup is depicted in Fig. 15 with the initial version of the ring light (v1: 36x LED type SFH4783, single board layout) shown in the left image and the revised ring light system (v2: 32x SFH4780S, quarter segment boards) shown on the right.

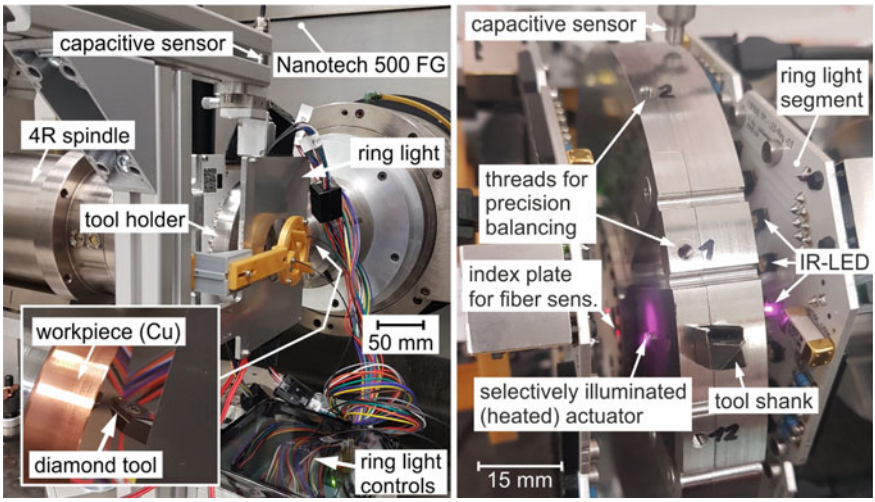

Fig. 15 Machine setup for evaluating the thermal tool holder on a Nanotech 500 FG. Left image shows the complete setup with ring light version 1 and the right image shows a closeup of the setup with the revised ring light (version 2)

6 Assessment of Actuator Performance

6.1 Results from Spindle Tests (No Machining)

When testing the actuator performance under rotation of the spindle, further processing of the measurement data is required. As the position of the reference plane is continuously measured during the process, the signal has to be segmented in order to reflect the position of the respective sections. A complete measurement of several revolutions as well as a zoom to a single revolution is shown in Fig. 16.

Due to the notches of the flexure hinges, the individual sections of the actuator are easily identifiable by the signal dropouts that occur when the capacitive measurements move out of the sensor's range at these points. Thus, they are utilized for the segmentation of the signal. The fully segmented signal consists of eight distinct sections: the two actuators, four flexure hinges (two per actuator) and two large portions in between. The latter should not be affected by the thermal state of the actuator and thus are used as reference. While the flexure hinges expand along with the thermal actuators, their position is of no relevance to the tool setting. However, their position could be evaluated to detect an asymmetry of the thermal expansion due to inhomogeneous heating as a result of misalignment between heat source and actuator.

In order to assess the temporal development of the thermal expansion, the mean position of each segment is determined for each revolution. Therefore, the noise of the signal is first reduced by applying a low-pass Butterworth filter with a cut-off

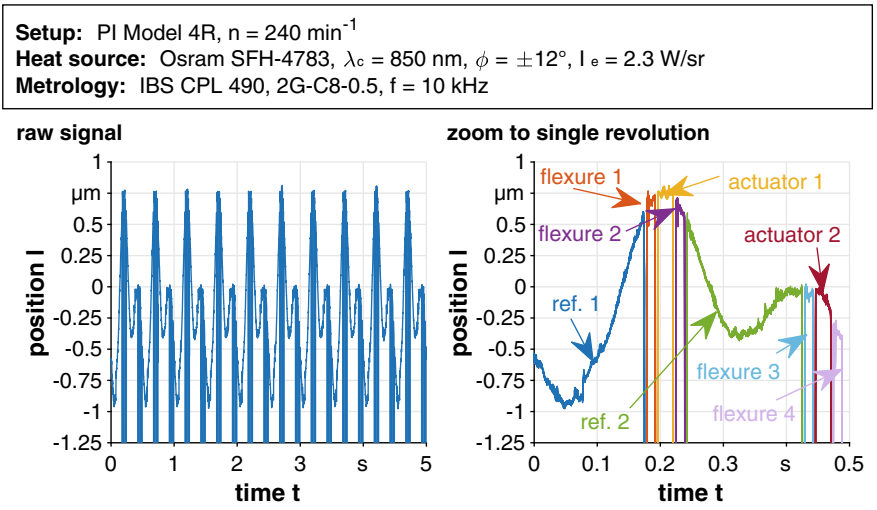

Fig. 16 Measurement of the reference plane with rotating spindle: raw data of 10 consecutive revolutions (left) and segmentation of a single revolution and association to actuator geometry (right)

frequency of $\lambda_c = 100$ Hz. Then, the mean signal of the first couple of revolutions is subtracted from each subsequent revolution in order to remove systematic deviations, like e.g. unbalances or runout errors, from the measurement. Finally, the segments are averaged into a single value which is recorded as the position of the respective segment. The temporal development of an exemplary test run at $n = 240$ min^{-1} is shown in Fig. 17.

Testing for the maximum thermal expansion that can be achieved at selected spindle speeds yields the following graph (Fig. 18).

This shows a clear dependence of the maximum expansion on the applied spindle speed that can be fitted to a logarithmic equation. The faster the speed is set, the more forced convection occurs on the actuator surface, resulting in a cooling of the thermal actuator and thereby a reduction of the maximum expansion. Nevertheless, up to a speed of $n = 1{,}500$ min^{-1} the achievable expansion is deemed sufficient to compensate most residual misalignment of the diamond tools after presetting.

6.2 Open-Loop Performance in Cutting

The tests in an test stand environment (i.e. without actual tool-workpiece interaction) have proven the general applicability of the selected method for tool setting on a rotating spindle. However, in this setup the location of the cutting edge is not determined directly, but measured as a shift of the reference plane situated slightly

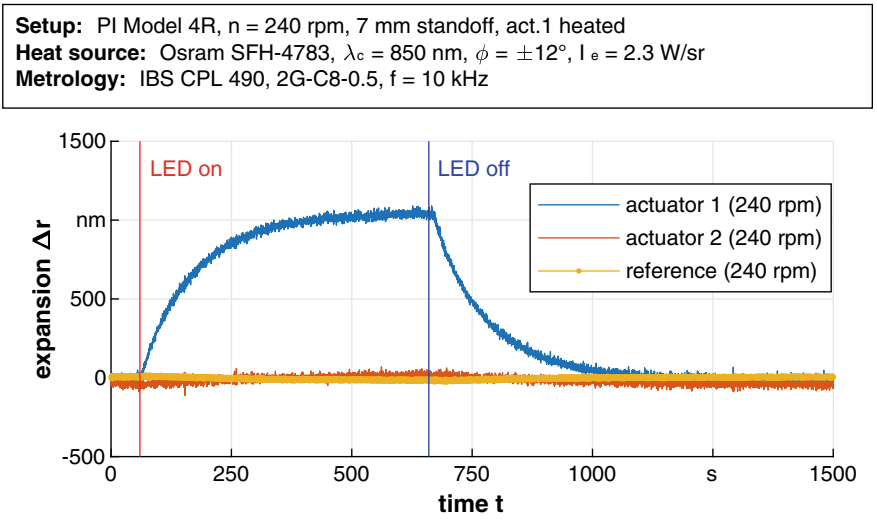

Fig. 17 Comparison of actuator expansion at 240 min^{-1} for a LED standoff distance of 7 mm; the light rings are switched to full power (1 A per active LED) between $t = 60$ s and 660 s

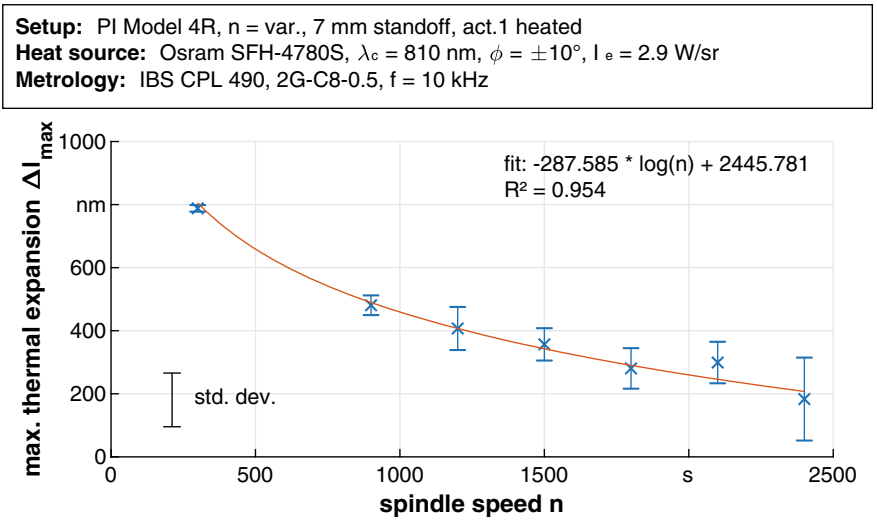

Fig. 18 Maximum thermal expansion for selected spindle speeds

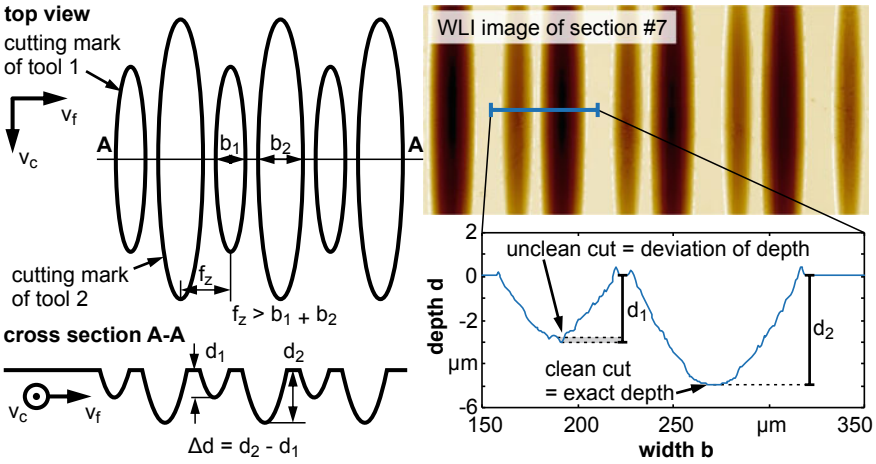

Fig. 19 Generation of isolated cutting marks from two engaged cutting edges by applying elevated cross feed velocity and measurement of generated marks with a WLI for evaluating the depth difference

below the tool shank on the circumference of the tool holder. Thus, it has to be verified whether the thermal expansion also affects the position of the cutting tool as a whole. This can only be analyzed in actual cutting experiments.

Therefore, a strategy was developed in which the tool inserts are mechanically pre-aligned. The infeed of the machine is set such that both cutting edges leave a mark on the surface of the workpiece (Fig. 19).

During cutting the cross feed velocity v_f is then set according to the selected spindle speed so that both tools leave separated marks on the workpiece surface. While heating the actuator with the LED ring light system, a set of these cutting marks is generated at selected time intervals (here: $\Delta t = 1$ s) to inscribe the respective state of the actuator expansion to the workpiece surface. This is later evaluated by measuring the cutting marks with a white light interferometer (WLI, a Talysurf CCI HD was utilized in this study) and determining the depth of the adjacent cutting marks. By comparing the development of the depth difference Δd to the initial state before heating the actuator, the thermal expansion $\Delta L = \Delta d$ of the tool holder is determined. The resulting measurements are shown in Fig. 20.

It can be seen that the mark depth changes according to the shift of the reference plane. However, the depth evaluation is prone to large deviations resulting from the depth measurements and the determination of the correct offsets. Furthermore, registration to the time-based measurements of the reference plane is done manually and thus associated with a deviation as well.

Nevertheless, a shift of the cutting edges along with the reference plane is observed for all measurements up to a spindle speed of $n = 1{,}800\ \mathrm{min}^{-1}$. Higher speeds could not be applied as the maximum feed velocity of the Nanotech 500 FG (max. $v_f = 600\ \mathrm{mm\ min}^{-1}$) is not sufficient to generate isolated marks in this case. Figure 21

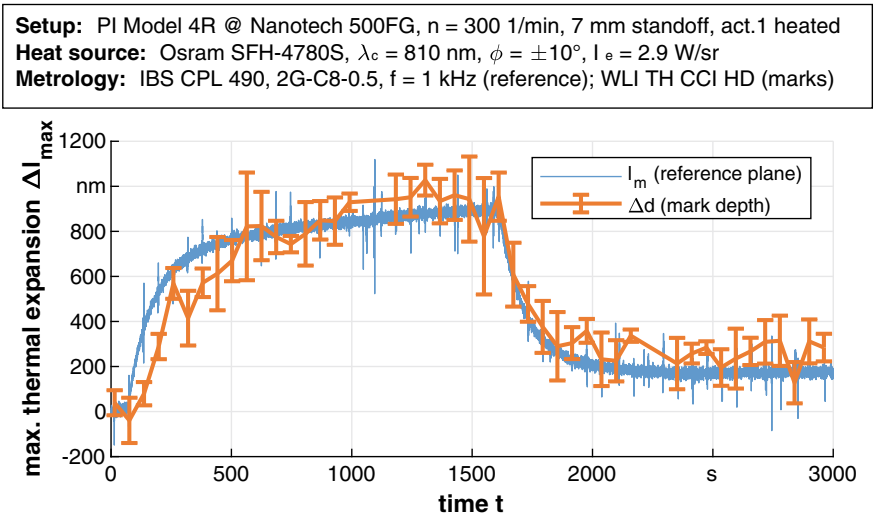

Fig. 20 Depth difference of cutting marks taken at 1 min intervals compared to the continuously measured expansion of the reference plane for $n = 300\ \mathrm{min}^{-1}$

shows a comparison of the maximum measured difference in mark depth to the maximum expansion of the reference plane. It can be observed that both curves follow the same trend with the expansion measured via the mark depth being slightly below that of the reference plane. Nevertheless, this is considered to be a systematic deviation of the actuator.

7 Control of Actuator Position to Nanometer Precision

The previous measurement have shown that the thermal actuator is generally capable of achieving the required expansion for compensating residual tool misalignment. However, in order to apply the system for the milling of an actual optical surface, the thermal expansion has to be precisely set within its range and this position has to be maintained throughout the whole cutting operation. Thus, a closed loop control of the thermal expansion has been implemented.

7.1 Design of Control Loop

The schematics of the (PI) control loop are shown in Fig. 22. The location of the reference plane l is measured by the capacitive sensor and compared to an initially selected offset L_0 to determine the thermal expansion ΔL_{meas}. This is then compared

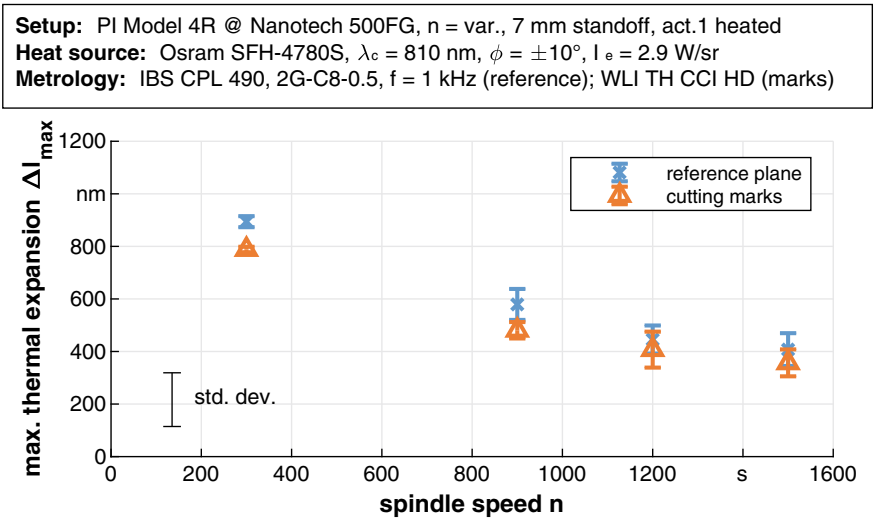

Fig. 21 Maximum thermal expansion of reference plane and depth difference of cutting marks for varied spindle speeds

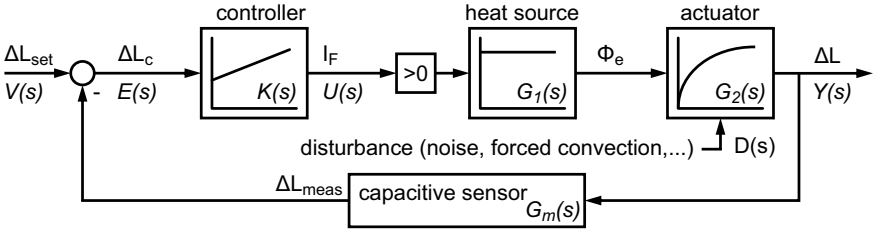

Fig. 22 Control loop for thermal expansion

to the set value of the expansion ΔL_{set} to determine the control offset ΔL_c. A proportional-integral-differential (PID)-controller is used to calculate the necessary forward current for the infrared LED I_f. This generates a radiant flux Φ_e that is directed on the actuator and causes a change of its temperature T_a. Due to the forced convection as a result of the spindle rotation, the actual temperature difference ΔT is reduced. Ultimately, this causes a thermal expansion ΔL of the actuator. Detailed explanations on the development of the control loop can be found in [12].

For the practical application, the sections of heat source, heat transfer, forced convection and actuator expansion are combined into a simplified model, i.e. a transfer function $G(s)$ of the whole system, which is derived from the step response $H(s)$ of the thermal actuator:

$$G(s) = \frac{Y(s)}{U(s)} = H(s) \cdot s \tag{5}$$

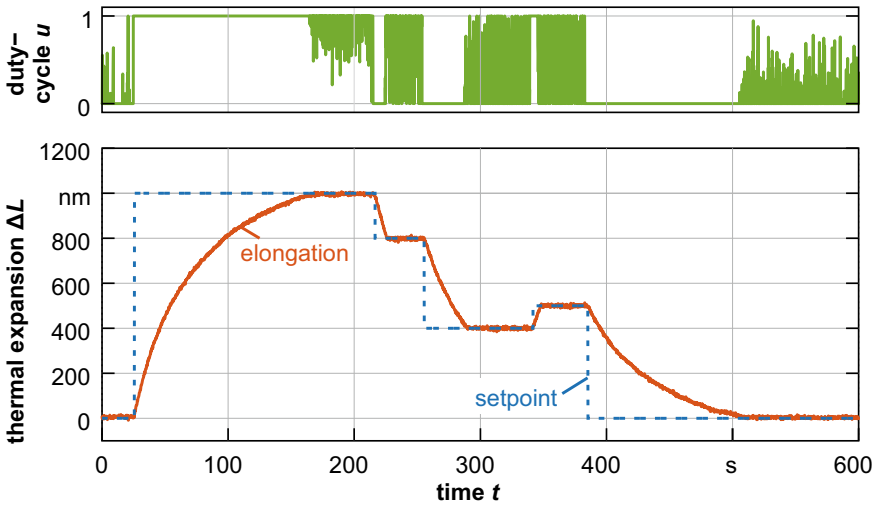

Fig. 23 Results for controlling the thermal expansion in a static setup

$$H(s) = \mathcal{L}\left\{\Delta L_{max} \cdot \left(1 - e^{-t/t_h}\right)\right\} \tag{6}$$

$$G(s) = \frac{\Delta L_{max}}{t_h \cdot s + 1} \tag{7}$$

7.2 Performance of the Control Loop in a Static Setup

Initially, the control loop was developed using a static setup of the actuator, to minimize disturbances from the dynamics of the spindle and to facilitate the acquisition of thermal expansion. With this setup it was verified that the thermal expansion may be controlled in the nanometer range and thereby be applied for tool setting. Figure 23 shows the system response for selected setpoints across the total range of thermal expansion. It can be seen that the targeted expansion is reached without overshoot and that a retraction of the actuator is possible by cooling the actuator (in this case by natural convection). The duty cycle of the LED still shows a lot of noise, which may be attributed to the not optimized control parameters chosen for this experiment.

In order to determine the minimum step size that can be set with the setup, a series of steps was fed to the control system, from ± 20 nm down to ± 1 nm. It is shown in Fig. 24 that steps down to ± 5 nm can be safely set within the system. While the 1 nm steps are also discernible in the graph, these set values cannot reliably be achieved, given the present measurement noise of approx. 6.5 nm.

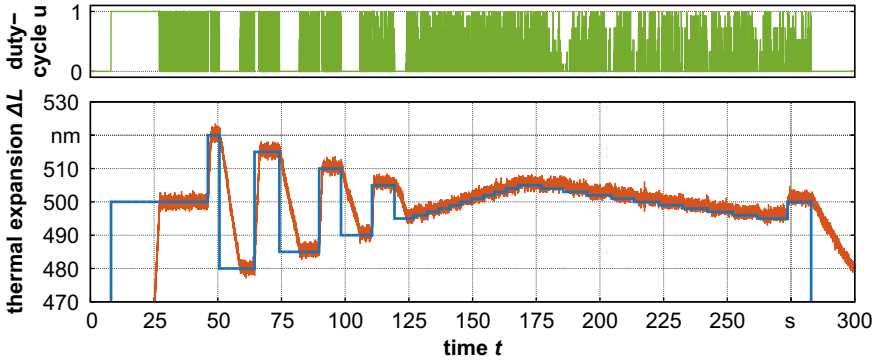

Fig. 24 Step series for determining the minimum control increments for the thermal actuator (static)

7.3 Performance of the Control Loop in a Spindle Setup

For control of the actuator during rotation of the spindle, its position has to be extracted from the roundness measurement of the reference plane. While this may be similarly done to the signal segmentation and analysis, the underlying approach is not suitable for real-time processing during the process. Instead, the position acquisition needs to be triggered per revolution so that only a small portion of the signal is processed (Fig. 25). In this case, the trigger signal is taken from the fiber optics measurement of the angular markings on the tool holder that are primarily used for advancing the LED of the ring lights.

On receiving a trigger signal, a finite number of samples with the selected frequency is acquired (Fig. 25, 1). For further processing and correct detection of all segments, the number of samples should be chosen so that one full revolution of the tool holder is obtained in one pass. For instance, at a typical sample rate of $f_s = 10$ kHz and a spindle speed of $n = 1{,}500$ min^{-1} (25 Hz), at least 400 samples are required. The measurement of a revolution is then aligned to a reference signal (2b), e.g. the mean of several revolutions with a defined heating state. After alignment, the signal dropouts are identified (3) and the data is split at these markers into sub-arrays representing each segment of the tool holder (4). To determine the average expansion of each segment, the difference between the current measurement and the reference is calculated (5) and the median of the resulting array is passed on (6). The median is preferred here over the mean of the segment, as it is more robust.

The extracted position of the actuator segment can then be utilized for building a control loop similar to that of the static setup. This has been done using a digital twin of the actual actuator that mimics its response (i.e. thermal expansion) to the control input (i.e. LED power) on the basis of a plant model (Fig. 26). In this way, the software implementation can be conducted truly independent of the availability of the setup on the machine tool. The internal plant parameters of the digital twin were calculated

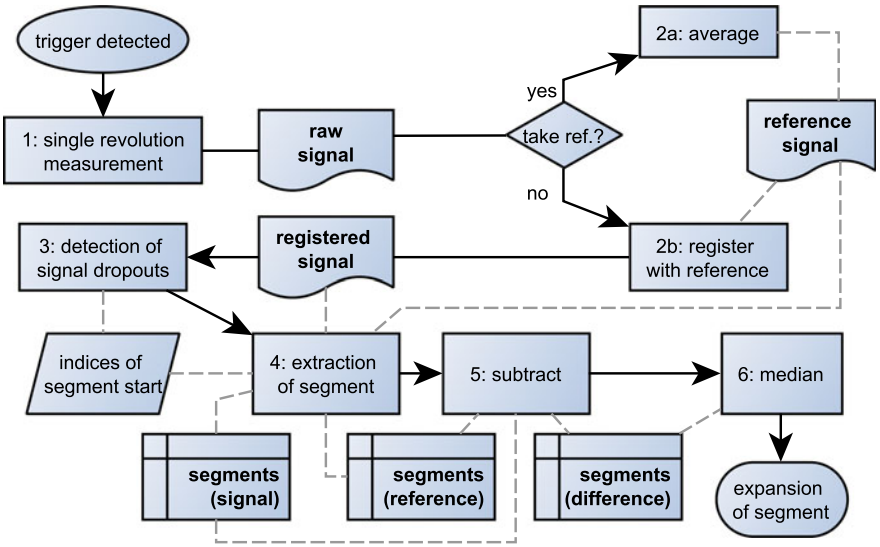

Fig. 25 Triggered data acquisition for determining position of actuator segment

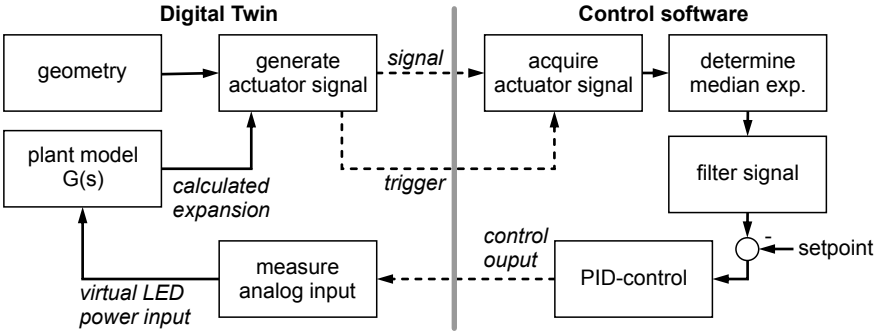

Fig. 26 Schematics of Digital Twin for the offline development of actuator controls

from the measurements obtained for the actual tool holder at $n = 240\ \text{min}^{-1}$, as shown in the previous sections ($K_{u,\text{DT}} = 1{,}102$ nm, $T_{i,\text{DT}} = 49.8$ s, $T_{d,\text{DT}} = 0.02$ s).

It has to be noted that while a spindle speed can be set within the digital twin, this only affects the frequency of the generated signal. The reduced maximum thermal expansion due to the forced convection is not considered in the current implementation, as it is not inherently necessary for the development of the control software. In the present evaluation, the plant model has been derived from a measurement of the actuator taken at low-speed, while the generation rate has been set to elevated spindle speed ($2{,}400\ \text{min}^{-1}$) to minimize the effective processing time of the simulations.

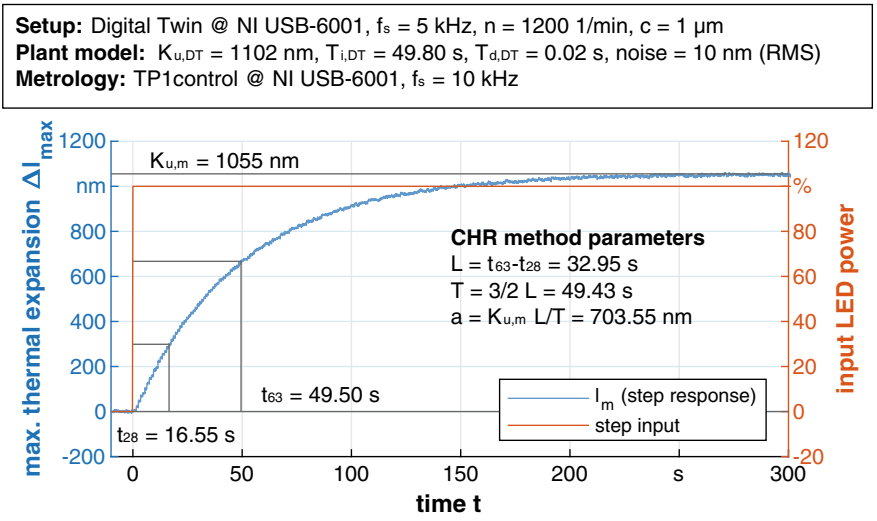

Fig. 27 Step response measured using a digital twin of the rotating tool holder and derived plant parameters

To account for possible deviations introduced by the signal splitting and the digital twin setup, the step response of the actuator is measured again with the adapted control software and the plant parameters of the actuator are determined (Fig. 27).

It can be seen that the measured plant parameters and are close to the respective parameters set in the digital twin ($K_{u,m} \approx K_{u,DT}$ and $T \approx T_{i,DT}$) with the dead time being significantly increased compared to the plant model $L \gg T_{d,DT}$. This is caused by expansion not being measured continuously, but once per revolution, i.e. at a significantly reduced frequency. Thus, the reaction of the system is measured later than the actual occurrence of the thermal expansion. Nevertheless, this is automatically considered by the control loop if the plant parameters are determined in this way.

The parameters for the PID controller are then calculated using different approaches. Initially, the method of (CHR) for setpoint accuracy with minimal overshoot was chosen and compared to the CHR calculation for disturbance rejection with minimal overshoot [5]. Additionally, the controller was tested with manually tuned parameters: K_p was chosen higher than the CHR values for potential decrease of rise time and steady-state error, T_i was set to a very long time constant as this is a major factor for decreasing the steady-state error and T_d was set to a small value for improved disturbance rejection. The calculated parameters are listed in Table 4.

The following Fig. 28 shows the response of the system with a closed control loop using the abovementioned PID parameters for a step-input of 500 nm. It can be seen that both parameter sets calculated according to the CHR method resulted in significant overshoot of the actuator position before settling to its final position. The method for setpoint accuracy yields less overshoot, but a significantly longer settling time than the other methods. With the parameters for disturbance rejection,

Table 4 Control parameters for the thermal tool holder (digital twin)

Parameter	CHR (setp. acc.)		CHR (dist. rej.)		Manually tuned	
	Calculation	Value	Calculation	Value	Calculation	Value
K_p	$0.6/a$	0.00085	$0.95/a$	0.00134	"High"	0.0064
T_i	$1 \cdot T$	49.43 s	$2.4 \cdot T$	119.16 s	"Very long"	1,200 s
T_d	$0.5 \cdot L$	16.48 s	$0.42 \cdot L$	13.9 s	"Short"	3 s

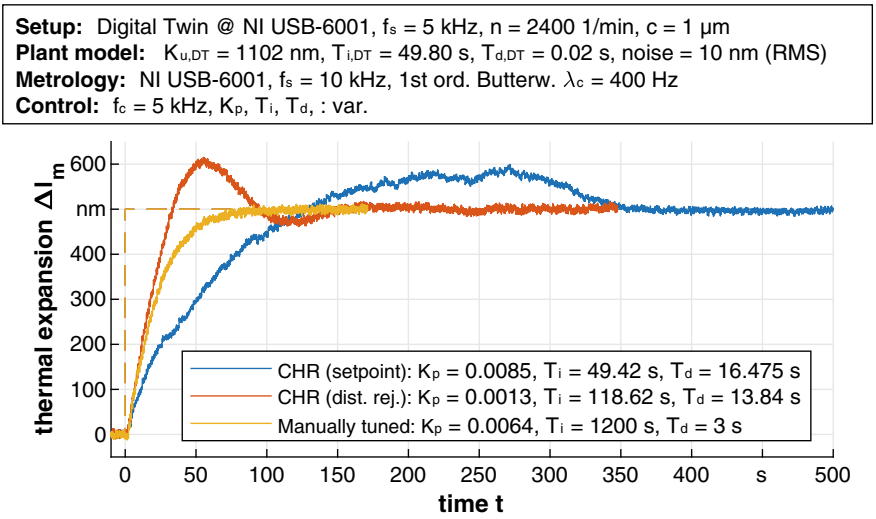

Fig. 28 Comparison of control parameters for a setpoint of 500 nm using a Digital Twin of the tool holder

the settling time is improved, but the overshoot is further increased. The self-tuned parameters yields the best results in terms of settling time, overshoot and setpoint accuracy and thus are chosen for further analysis.

The controlled response of the system using the self-tuned parameters is applicable across the complete stroke of the actuator as is shown in Fig. 29. As there is no overshoot with these parameters, the system may well be utilized for in-process re-setting of the tool, e.g. to compensate for gradual tool wear or low-dynamic disturbances.

With the given noise of the system (10 nm RMS), the system follows inputted setpoints down to ±5 nm, as depicted in Fig. 30.

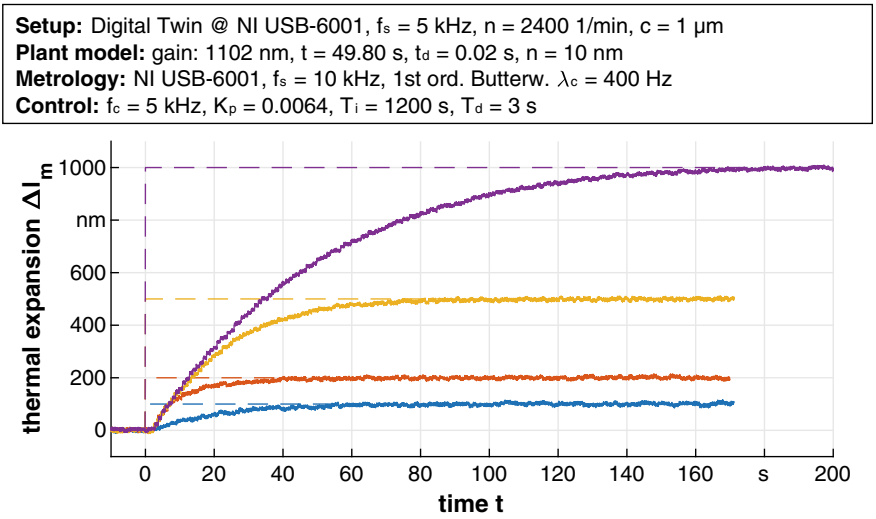

Fig. 29 Closed loop control of actuator position (Digital Twin) for selected setpoints

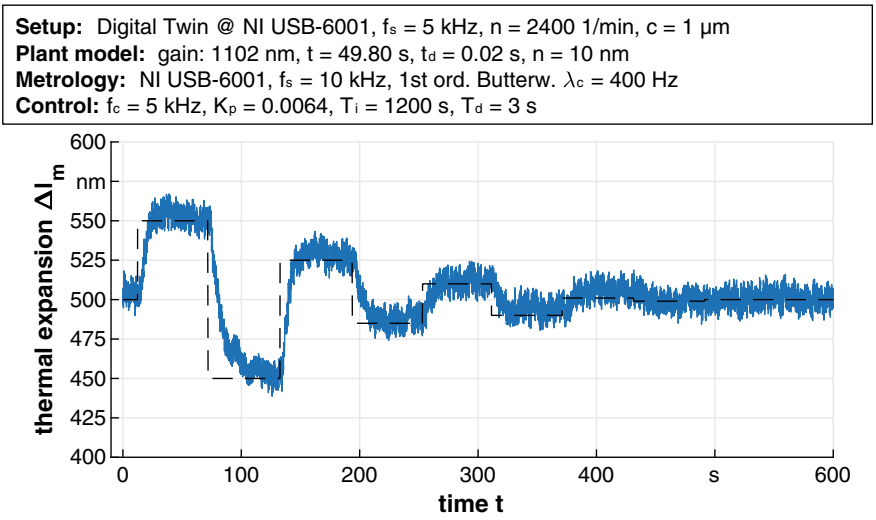

Fig. 30 Control response (Digital Twin) for selected small scale setpoints

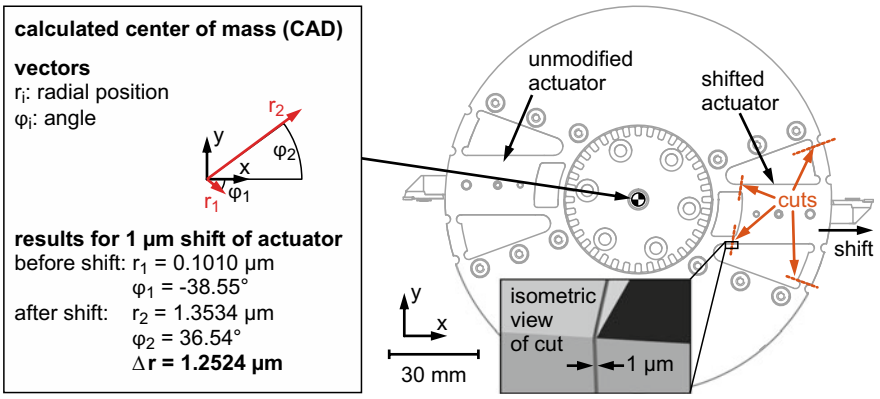

Fig. 31 Calculated unbalances for thermally expanded actuator

8 Influence Multi-tool-holder on General Machining Performance

After the control of the thermal actuator has been successfully demonstrated, this section will focus on potential influences of the tool-holding mechanism on the process itself.

8.1 Impact of Tool-Shift on Unbalances

First, it has been examined whether the tool shift induced by the thermal actuator results in a change of the balancing state of the rotor. Calculations based on the CAD model indicate that shifting one of the actuators by its maximum expansion (1 µm) moves the center of mass of the tool holder by approximately 1.25 µm (see Fig. 31). In theory, this results in a measurable change of the balancing state and could potentially be applied for ultra-fine balancing of the rotor, if a compensation mass is shifted in this way.

In order to verify this, the balancing state was measured experimentally for selected spindle speeds with the actuator at its base length ("cold") and at its maximum expansion ("heated"). The results are shown in Fig. 32. Generally, the measured unbalance is decreasing with increasing spindle speed. While the mean unbalance is approx. 5 g mm at 900 min^{-1}, it is below 0.31 g mm at 2,500 min^{-1}. Furthermore, no significant change of the unbalance could be detected when the actuator is at its maximum thermal expansion. This also implies that the system cannot be applied for balancing purposes in its current form.

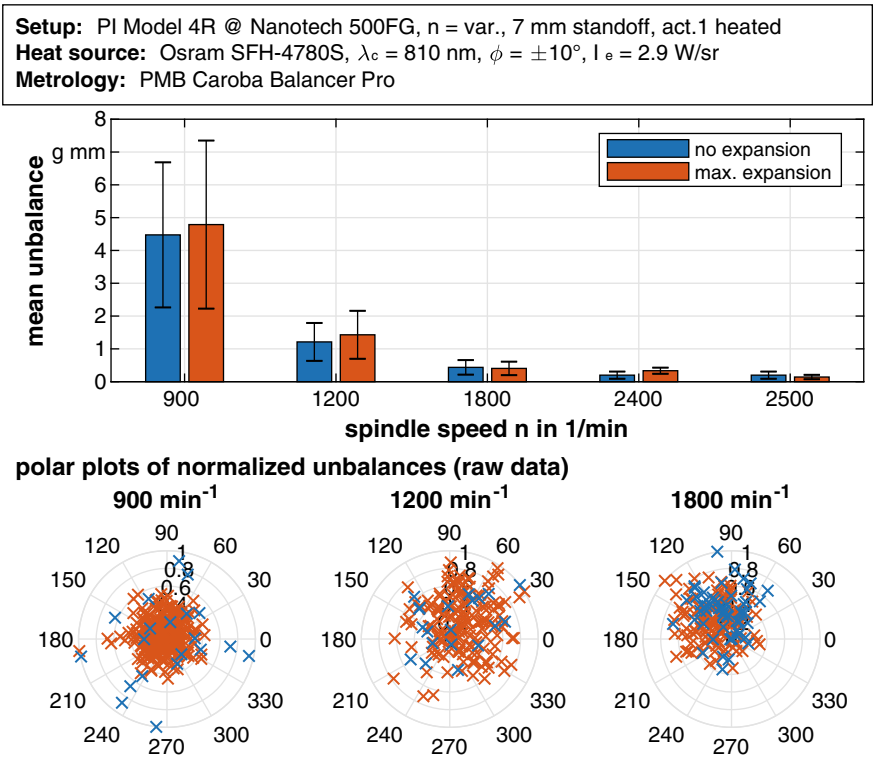

Fig. 32 Effect of tool setting on unbalances: mean unbalance and standard deviation for cold actuator and maximum thermal expansion (top) and normalized unbalances for selected spindle speeds (bottom)

8.2 Influence of Spray Mist Lubricant on Thermal Tool Setting

In the final experiments of this study, the influence of cutting fluid on the performance of the thermal tool setting was analyzed. For this, the cutting experiments described in Sect. 6.2 were repeated with minimum quantity lubrication directed at the cutting zone. The resulting spray mist potentially covers the heated faces of the actuator, thereby cooling the substrate in addition to the forced convection by the spindle rotation. Paraffin oil was selected as cooling fluid for these experiments, because it is electrically non-conductive and thus will not influence the electronics of the ring light system. In addition, it is only applied locally at the tool-workpiece contact point and therefore the influence of capacitive measurement of the reference plane is minimized. An exemplary analysis of both, the expansion measured at the reference plane and the cutting mark depth evaluated from the surface measurements, is shown in Fig. 33.

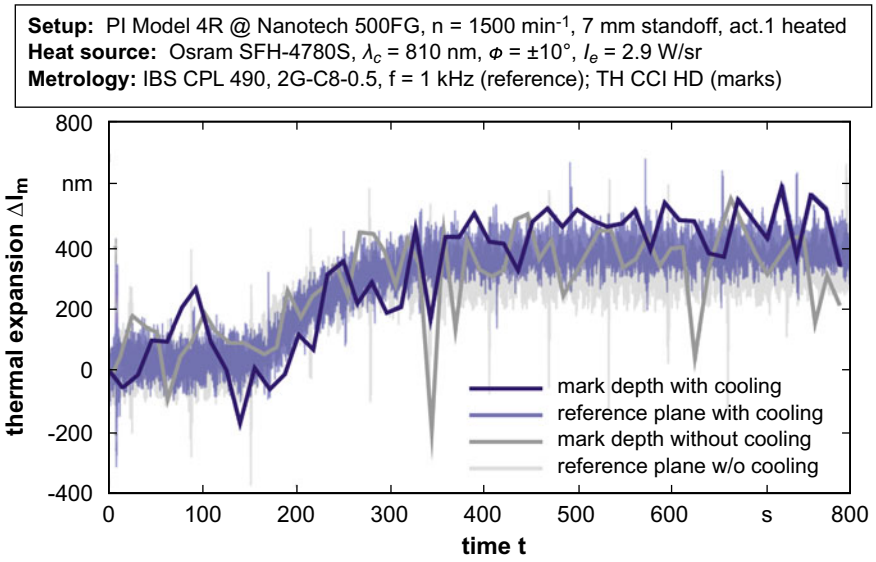

Fig. 33 Measured expansion of the thermal tool holder (reference plane) and depth change of cutting marks (actual tool shift) for cutting tests with and without cooling fluid

The analysis shows no measurable reduction in actuator expansion and tool shift for machining with cutting fluid. Both parameters indicate an expansion of 400 nm that is achieved after about 400 s.

9 Conclusion and Outlook

Diamond milling using multiple cutting edges offers the potential to significantly increase the productivity of diamond machining. Its broad application is averted by the lack of ultra-precision tool setting mechanisms that can be applied on rotating spindles. Hence, the possibility of a thermally induced tool setting was investigated in this study. By locally heating a specific section of the milling tool, i.e. the tool holder, an actuating mechanism was triggered that causes the attached diamond tool and its cutting edge to shift in radial direction. A closed loop control can then be applied to minimize the deviation between this tool's radius and that of other tools in the setup.

The thermal actuating mechanism was initially analyzed using finite element modeling and later evaluated a static test stand. Based on the findings obtained in these studies, a final design of a milling tool with thermally adjustable holders for two diamond tools was derived. The heat input is generated by a moving ring light with infrared LED which has been specifically designed for this purpose (patent pending).

Additional tests of the novel milling tool on spindle test stands and in machining experiments have confirmed the general applicability of thermal tool setting in diamond milling. It was possible to build a closed loop control of the thermal actuator that evaluates the position of a reference plane during rotation and drives the ring light according to the determined offset. The initial parameterization of the control loop yields acceptable results in terms of setpoint accuracy and speed, but still results in overshoot of the expansion. Thus, an optimized controller using manually tuned parameters has been derived using a Digital Twin of the system. The controller drives the actuator to its maximum expansion in about 200 s and achieved a setpoint accuracy of ±5 nm. Furthermore, it has been demonstrated that the thermal tool setting does not change the balancing state of rotor and even is unaffected by spray mist lubrication of the cutting zone.

In order to mature this concept to an industrially applicable solution, a further analysis of the position stability and repeatability as well as of the impact of the localized heating on the long-term thermal stability of the machine tool is vital. Furthermore, the electronics, software and (setup-)procedures have to be refined in order to be applicable in an industrial environment.

References

1. Bono, M., Hibbard, R.: A flexure-based tool holder for sub-μ positioning of a single point cutting tool on a four-axis lathe. Precis. Eng. **31**(2), 169–176 (2007). https://doi.org/10.1016/j.precisioneng.2006.03.007
2. Brinksmeier, E., Gläbe, R., Autschbach, L.: Novel ultraprecise tool alignment setup for contour boring and ball-end milling. In: 18th ASPE Annual Meeting, Portland/Oregon, USA, October 2013, pp. 271–274. American Society for Precision Engineering (2013)
3. Brinksmeier, E., Preuss, W.: Micro-machining. Philos. Trans. Roy. Soc. A **370**, 3973–3992 (2012). https://doi.org/10.1098/rsta.2011.0056
4. Brinksmeier, E., Riemer, O., Gläbe, R.M. (eds.): Fabrication of Complex Optical Components. Springer, Heidelberg (2013). https://doi.org/10.1007/978-3-642-33001-8
5. Chien, K.L., Hrones, J.A., Reswick, J.B.: On the automatic control of generalized passive systems. Trans. ASME **74**, 175–185 (1952)
6. Dornfeld, D., Min, S., Takeuchi, Y.: Recent advances in mechanical micromachining. CIRP Ann. **55**(2), 745–768 (2006). https://doi.org/10.1016/j.cirp.2006.10.006
7. Fang, F.Z., Zhang, X.D., Weckenmann, A., Zhang, G., Evans, C.J.: Manufacturing and measurement of freeform optics. CIRP Ann. **62**(2), 823–846 (2013). https://doi.org/10.1016/j.cirp.2013.05.003
8. Neugebauer, R., Denkena, B., Wegener, K.: Mechatronic systems for machine tools. CIRP Ann. **56**(2), 657–686 (2007). https://doi.org/10.1016/j.cirp.2007.10.007
9. Schönemann, L., Brinksmeier, E., Osmer, J.: A piezo-driven adaptive tool holder for ultraprecision diamond tool alignment. In: van Brussel, H., Brinksmeier, E., Spaan, H., Burke, T. (eds.) 9th Euspen International Conference, vol. 1, pp. 398–401 (2009)
10. Schönemann, L., Mejia, P., Riemer, O., Brinksmeier, E.: Design and evaluation of a thermal actuator for ultra-precision machining. In: Blunt, L. (ed.) 11th International Conference & Exhibition on Laser Metrology, Machine Tool, CMM & Robotic Performance (Lamdamap 2015), pp. 320–330. Euspen (2015)

11. Schönemann, L., Preuss, W., Riemer, O., Foremny, E., Brinksmeier, E., Kuhfuss, B.: Ultrapräzise Hochgeschwindigkeitsbearbeitung. Teil 1: Steigerung der Flächenleistung durch den Einsatz von Mehrfach- Werkzeugen und HSC-Spindeln. wt Werkstattstechnik **105**(6), pp. 366–370 (2015)
12. Schönemann, L., Riemer, O., Brinksmeier, E.: Control of a thermal actuator for UP-milling with multiple cutting edges. Procedia CIRP **46**, 424–427 (2016). https://doi.org/10.1016/j.procir.2016.03.194. Ed. by Wertheim, R., Ihlefeldt, S., Hochmuth, C., Putz, M
13. Schönemann, L., Riemer, O., Brinksmeier, E.: Arbeitsmaschine mit einem rotierenden Maschinenteilhalter, insbesondere Werkzeugmaschine mit rotierendem Werkzeughalter, Verfahren zum Justieren eines Maschinenteils, insbesondere Werkzeugs, sowie Ringlicht für eine derartige Arbeitsmaschine. German pat. req. 10 2017 119 828 A1. Leibniz-Institut fürWerkstoforientierte Technologien IWT, Universität Bremen, 29 August 2017
14. Schönemann, L., Riemer, O., Brinksmeier, E.: Recent advances in ultra-precision milling with multiple-cutting edges. In: 32nd ASPE Annual Meeting, Charlotte/NC, USA, 29 October–3 November 2017, pp. 175–179. American Society for Precision Engineering (2017)
15. Schönemann, L., Riemer, O.: Thermo-mechanical tool setting mechanism for ultra-precision milling with multiple cutting edges. Precis. Eng. (2018). https://doi.org/10.1016/j.precisioneng.2018.09.003
16. Schönemann, L.: Surface simulation for ultra-precision milling with multiple cutting edges. In: 69th CIRP General Assembly - Part 2, Birmingham, 22 August 2019
17. Schönemann, L., Berger, D., Dörgeloh, T., Riemer, O., Brinksmeier, E., Krüger, R., Schreiber, P., Denkena, B., Hochbein, J., Parsa, N., Schenck, C., Kuhfuss, B.: Synergistic approaches to ultra-precision high performance cutting. CIRP J. Manuf. Sci. Technol. **28**, 38–51 (2020). https://doi.org/10.1016/j.cirpj.2019.12.001
18. Sortino, M., Totis, G., Kuljanic, E.: Comparison of injection molding technologies for the production of micro-optical devices. Procedia Eng. **69**, 1296–1305 (2014). https://doi.org/10.1016/j.proeng.2014.03
19. Sze-Wei, G., Han-Seok, L., Rahman, M., Watt, F.: A fine tool servo system for global position error compensation for a miniature ultra-precision lathe. Int. J. Mach. Tools Manuf. **47**(7–8), 1302–1310 (2007). https://doi.org/10.1016/j.ijmachtools.2006.08.023
20. Transregionaler Sonderforschungsbereich TR4, ed. Prozessketten zur Replikation komplexer Optikkomponenten. Abschlussbericht. Berichtszeitraum 7/2008–8/2012 (2012)
21. Zhang, S.J., To, S., Zhu, Z.W., Zhang, G.Q.: A review of fly cutting applied to surface generation in ultra-precision machining. Int. J. Mach. Tools Manuf. **103**, 13–27 (2016). https://doi.org/10.1016/j.ijmachtools.2016.01.001